Optimal Configuration of Proton-Therapy Accelerators for Relative-Stopping-Power Resolution in Proton Computed Tomography

Alexander T. Herrod,[1,2,*] Alasdair Winter,[3] Serena Psoroulas,[4] Tony Price,[3] Hywel L. Owen,[2,5,†] Robert B. Appleby,[1,2,‡] Nigel Allinson,[6] and Michela Esposito[6]

[1] *University of Manchester, Manchester, United Kingdom*
[2] *The Cockcroft Institute, Daresbury, United Kingdom*
[3] *University of Birmingham, Birmingham, United Kingdom*
[4] *Paul Scherrer Institut, Villigen, Switzerland*
[5] *STFC Daresbury Laboratory, Daresbury, United Kingdom*
[6] *University of Lincoln, Lincoln, United Kingdom*

(Received 5 November 2021; accepted 5 May 2022; published 11 July 2022)

The determination of relative stopping power (RSP) via proton computed tomography (pCT) of a patient is dependent in part on the knowledge of the incoming proton kinetic energies; the uncertainty in these energies is in turn determined by the proton source—typically a cyclotron. Here, we show that reducing the incident proton beam energy spread may significantly improve RSP determination in pCT. We demonstrate that the reduction of beam energy spread from the typical 1.0% (at 70 MeV) down to 0.2% can be achieved at the proton currents needed for imaging at the Paul Scherrer Institut 250-MeV cyclotron. Through a simulated pCT imaging system, we find that this effect results in RSP resolutions as low as 0.2% for materials such as cortical bone, up to 1% for lung tissue. Several materials offer further improvement when the beam (residual) energy is also chosen such that the detection mechanisms used provide the optimal RSP resolution.

DOI: 10.1103/PhysRevApplied.18.014020

I. INTRODUCTION

Proton computed tomography (pCT) is a technique that promises to help realize the full benefits of proton therapy [1,2], by imaging patients prior to treatment with a sparse proton beam from the same particle source used for treatment. The use of pCT improves knowledge of proton dose deposition beyond that offered by conventional x-ray CT scans (largely due to the latter requiring the conversion from Hounsfield units to relative stopping power, RSP [3]), as well as providing imaging on the same machine as treatment is performed (potentially not having to move a patient between scanning and treatment).

A pCT measurement typically follows the passage of a large number ($>10^8$) of individual protons through a heterogeneous region, building an image from the difference between the incident and final measured energy of each proton. Contributions to uncertainties in the measured depths and densities that protons have traversed in the patient, and properties of the incident protons, increase the overall uncertainty of the imaging. Hence, these contributions should be individually considered and reduced.

Previous studies have utilized the same energy spread as used in treatment to maximize dose rate whilst maintaining an acceptable spread of the Bragg peak.

Here, we consider how a smaller incident energy spread may benefit proton energy determination during pCT. We investigate contributions to the RSP uncertainty in cortical bone, rib bone, adipose, lung tissue, water (materials relevant for head and neck imaging), and PMMA (acrylic), both due to the energy spread of the incident proton beam and from the choice of incident energy.

A separate recent study [4] has examined how varying the incident energy can remove imaging artefacts. Here, we propose that the RSP resolution can be optimized by reducing the incident proton beam energy spread, in combination with careful choice of incident proton energy. We start by showing—using measurements performed at the Paul Scherrer Institut (PSI) PROSCAN facility—that a 0.2% incident beam energy spread is reliably achievable.

We then describe the simulations used to perform the investigations in Sec. III, with which both beam energy spread (discussed in Sec. IV A) and residual energy (in Sec. IV B) are optimized. The results of both optimizations

*alexander.herrod@cockcroft.ac.uk
†hywel.owen@stfc.ac.uk
‡robert.appleby@manchester.ac.uk

are summarized in Sec. V, with clear improvements in RSP resolution found.

II. PRACTICAL DEMONSTRATION OF REDUCED BEAM ENERGY SPREAD AT PSI

An investigation is performed [5] at the COMET cyclotron at PSI [6], where the energy-selection collimator aperture is reduced to provide an energy spread of 0.1%. The energy spread of the beam is then measured at the isocenter.

A water range telescope, consisting of a movable tracker within a water tank shown in Fig. 1, is used to find the position and width of the Bragg peak at beam energies of 70 and 230 MeV, as described in Ref. [7]. The Bortfeld model [8] is used to fit the dose deposition data from the range telescope as in Fig. 2, and so find the energy spreads of the beam.

It is found that beam currents between 20 and 100 pA, sufficient for pCT scans, can be maintained with the reduction of beam energy spread to 0.2%, for the full energy range (70–250 MeV). Smaller energy spreads cannot be achieved reliably, due to mechanical limitations in the beamline momentum spread selection collimator.

Standard beam energy spreads for treatment with this machine are shown in Table I, along with the achievable 0.2% spreads.

We suggest that the reduced fractional beam energy spread at higher energy (top-right of Table I) is due to reduced use of the beam energy absorber, which spreads, as well as reduces, the proton energies.

Hence, in the case where the beam is used for pCT scans, this energy spread can be reduced with a (desired) reduction in beam current, allowing for simpler proton tracking hardware and processing. We expect the most substantial improvement in resolution at lower beam energies, where the relative improvement in beam energy spread is greater.

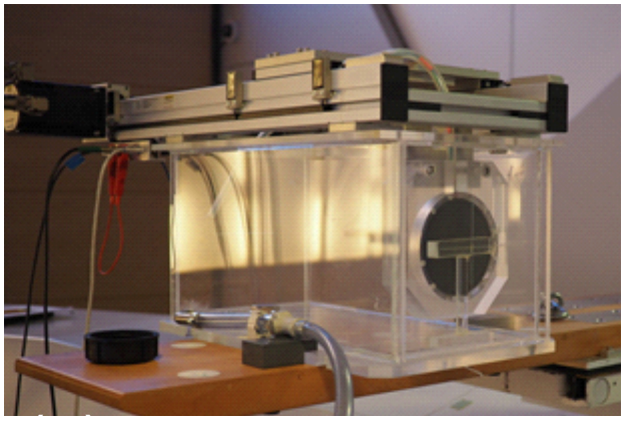

FIG. 1. The water range telescope used for the estimation of the minimum energy spread achievable in the clinical beam line at PSI Gantry 2.

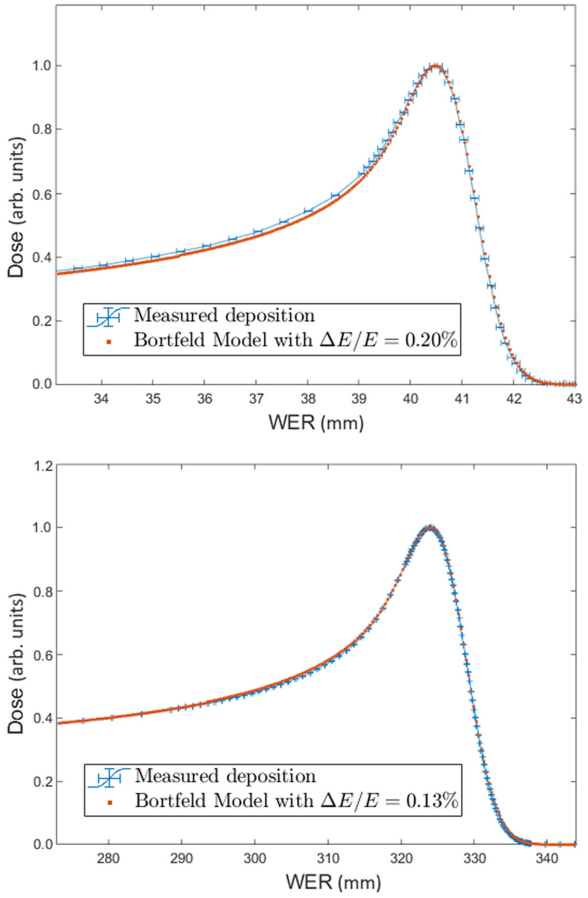

FIG. 2. Measured proton dose deposition in the water range telescope at PSI for minimum beam energy spread, compared with the fitted Bortfeld model for 70 MeV (top) and 230 MeV (bottom). The widths of the Bragg peaks are fitted to determine energy spread; the resulting dE/E is extracted with a precision of 5%–10% depending on the energy.

To quantify these improvements, we investigate reductions in energy spread with our simulations.

III. SIMULATION OF PHANTOM pCT IMAGE RECONSTRUCTION

Proton CT scans require knowledge of the direction and energy of protons entering and exiting an imaged object, represented here by a heterogeneous phantom. A typical pCT system consists of a set of proton trackers both before

TABLE I. A subset of manufacturer-specified beam energy spreads of the PSI treatment beam, and the 0.2% available on the same machine at lower currents for, e.g., pCT scanning.

Beam energy (MeV)	70	100	150	200	245
Beam energy spread (%)	1.1	1.1	0.9	0.6	0.3
Beam energy spread (MeV)	0.8	1.1	1.3	1.2	0.8
0.2% of beam energy (MeV)	0.1	0.2	0.3	0.4	0.5

and after the phantom to measure the incoming and outgoing proton trajectories, and an energy measurement device to measure the residual proton energy; the latter is often a range telescope based on scintillators.

In this paper, we develop a detailed GEANT4-based model (v10.0p4, physics list QGSP_BIC_EMY) of one potential tracking solution. We use this to perform a virtual pCT of a phantom using a scanned pencil beam with specifications representative of those of the research beamline at the Christie Hospital proton therapy center in Manchester (UK) based around a Varian PROBEAM cyclotron with notional fixed extraction energy of around 250 MeV, which is broadly similar to the Paul Scherrer Institut PROSCAN facility and many other high-intensity cyclotrons used for particle therapy. The GEANT4 model includes the effects of the beam, direction trackers, and phantom; the resolution in the energy measurement is implemented by smearing the true residual energy of each exiting proton according to a parameterization of the expected energy resolution as a function of proton energy.

To reconstruct a pCT image of our example phantom (detailed below), we consider 360 projections in steps of 1°; each projection uses 1×10^6 protons to uniformly irradiate an area of 8×8 cm^2, giving a total of 360×10^6 initial protons. The reconstructed trajectory and energy of the simulated protons are used to reconstruct an image using the backprojection-then-filtering method outlined in Ref. [9].

A. Phantom

In simulation we replicate the experimental phantom used by the PRaVDA collaboration for earlier pCT studies [10]; this is a spherical PMMA phantom with radius of 37.5 mm, containing two sets of three parallel cylinders (of 7.5-mm radius and 15-mm length), each made of a different tissue-equivalent material: cortical bone, rib bone, adipose, water, lung, and air. Two tungsten carbide balls of radius 0.5 and 1.0 mm are also embedded at one end of the phantom. The phantom is depicted in Fig. 3, showing the materials and relative positions of the cylinders and tungsten carbide balls.

When calculating the RSP resolution for each insert, only the central region ($r = 2.5$ mm, $Z = 7.5$ mm) is considered so as to avoid spatial resolution effects that arise at material boundaries, particularly at lower energies (a method common among CT RSP studies [11,12]).

B. Direction detection

The direction detection of the protons is based on using four silicon tracking modules as depicted in Fig. 4: a pair of modules upstream of the phantom measure the incident proton trajectories, and another pair of modules downstream of the phantom measure the exit proton trajectories. Each tracking module is similar to those described in Ref. [13], and contains a 600-μm total thickness of silicon strips with binary readout.

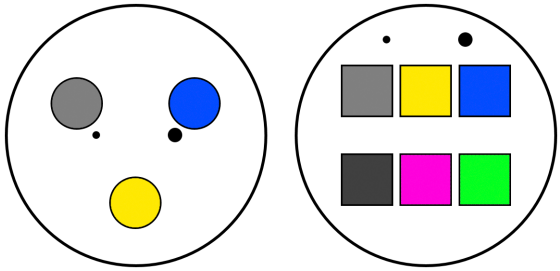

FIG. 3. The 75-mm-diameter phantom used in simulations, representative of the experimental PRaVDA phantom: a PMMA sphere contains six cylinders of cortical bone (dark gray), lung (pink), air (green), rib bone (light gray), adipose (yellow), and water (blue) and with two balls of tungsten carbide (black). The sphere is depicted viewed from above (left image) and from the side (right image).

Two of these tracking modules, separated by 100 mm, are situated upstream and two downstream of the phantom center, with a gap of 320 mm between the centers of the second and third modules to accommodate phantoms of up to 220 mm in diameter. The energy measurement device is immediately downstream of the final tracker. The average position taken from the planes in each tracker is used for reconstruction.

The silicon layers cause some multiple Coulomb scattering (MCS) and energy loss within the trackers. The two most important contributions from this are: MCS from the last Si layer of the upstream module pair reduces the accuracy with which the trajectory into the phantom is known; MCS from the first Si layer of the downstream module pair reduces the accuracy with which the trajectory exiting the phantom is known.

While the tracker can be optimized to deal with multiple simultaneous protons, here we only present results based on currents where there is only ever a single proton in the system at a time, to remove any complications due to tracking ambiguities.

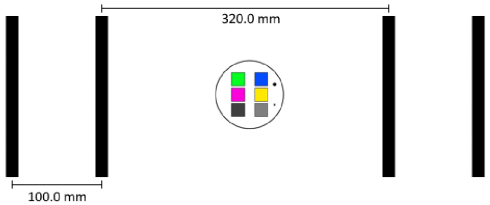

FIG. 4. Diagram of the direction tracker configuration used. Two trackers, each consisting of 600 μm of silicon, are situated upstream of the phantom, and two are situated downstream. The phantom sits in the center of a 320.0-mm separation between the centers of the innermost trackers.

TABLE II. Fractional energy measurement resolution at different energies in the range used for proton therapy, as determined from simulations. For the imaging simulations in Sec. III, these are approximated using the fit in (1). We include the corresponding water-equivalent thickness (WET) uncertainty at each energy, which improves at lower energy, suggesting that the fractional energy resolution is a poor indicator of performance for pCT.

Proton energy (MeV)	50	100	150	200	250
Measurement uncertainty (%)	2.8	0.95	0.75	0.70	0.68
Measurement uncertainty (MeV)	1.4	0.95	1.1	1.4	1.7
WET uncertainty (mm)	1.1	1.3	2.1	3.1	4.4

Further effects such as strip noise, charge diffusion between strips, dead regions, detector acceptance, and secondary particle production have been included in the study and are found to have minimal impact on the measured RSP resolution.

C. Energy detection

Different technologies may be used for the residual energy measurement in pCT. Here, we model the energy measurement in two ways. In the first, we parameterize the fractional energy resolution (in percent) of the calorimeter device detailed in Ref. [14] by

$$\sigma_{E\%} = \frac{146\,594}{E^{2.847\,57}} + 0.658\,351, \tag{1}$$

for which we present the energy resolutions in Table II.

For the imaging simulations in Sec. III, the fit in (1) is used to interpolate the energy resolution for intermediate energies.

In the other energy measurement method, we consider a hypothetical device with perfect energy measurement resolution, for which the true proton energies are used for reconstruction.

IV. SIMULATION RESULTS

Using the energy resolutions shown in Table II in the simulations described in Sec. III, we obtain the RSP values for imaging of cortical bone, adipose, rib bone, PMMA, water, and lung tissue. The initial beam energies used for these simulations are 230 and 130 MeV, with beam energy spreads of 0.2%, and of the treatment beam, at both energies.

Due to not all simulated protons striking the phantom, we note the mean residual energies of those that do. For the 230-MeV beam, this mean is 200 MeV, and is 85 MeV for the 130-MeV beam, suggesting a 50% increase in average dose at the lower energy. However, we also note that the use of a spherical phantom results in a wide variation in residual energy between protons striking the phantom tangent to the surface (traversing only a few millimeters before exiting) and those striking perpendicular to the surface (traversing the full diameter).

The 230-MeV simulations produce the highest reconstruction rates at 91% of the 360×10^6 simulated protons, which reduces to 81% for 130 MeV. This exposes our reason for not instead choosing a beam energy lower than 130 MeV: residual protons would undergo severe scattering, which reduces the accuracy and efficiency of the tracking, and increases the path uncertainty due to multiple scattering within the phantom.

We show the resulting RSP resolutions from the simulations in Fig. 5(b), for both initial beam energies of 230 and 130 MeV, with energy spreads of 0.2%. We also show these results for a perfect (0%) residual energy measurement resolution in Fig. 5(a).

A. Reducing beam energy spread

Reduction of the beam energy spread can only result in improvements for pCT, as the energies of individual protons (within the same bunch) before they enter the phantom can be known to higher accuracy. For all beam energies, the results from Sec. II indicate an available reduction in uncertainty of individual proton energy for all beam energies used, as compared with a treatment beam.

By reducing the beam energy spread in the simulations to the achievable value of 0.2%, we obtain the simulation results in Fig. 5(a) for a perfect energy detection resolution. Introducing the energy detection resolutions in Table II, we obtain the results in Fig. 5(b).

We see that the predicted RSP resolution improvement persists for both the 130- and 230-MeV beam energies studied. By removing the uncertainty in the residual energy measurement, we find Fig. 5(a) more clearly illustrates the improvement.

B. Optimizing residual energy

The choice of energy for a pCT scan should reflect the ideal combination of spatial resolution (not discussed or optimized here) and RSP resolution. Due to the WET uncertainty of the energy measurement improving at lower energies (Table II), one would expect a lower energy to provide a better RSP resolution, down to energies where the worsening spatial resolution forbids study of a heterogeneous phantom.

For the case of a perfect energy measurement, for beams of different energies with the same fractional energy spread [0.2% energy spread in Fig. 5(a)], we find that the beam of lower energy provides an improvement in RSP resolution over the 230-MeV beam for all materials.

However, this behavior is not as consistently observed in the results incorporating a residual energy measurement uncertainty, indicating that the energy measurement

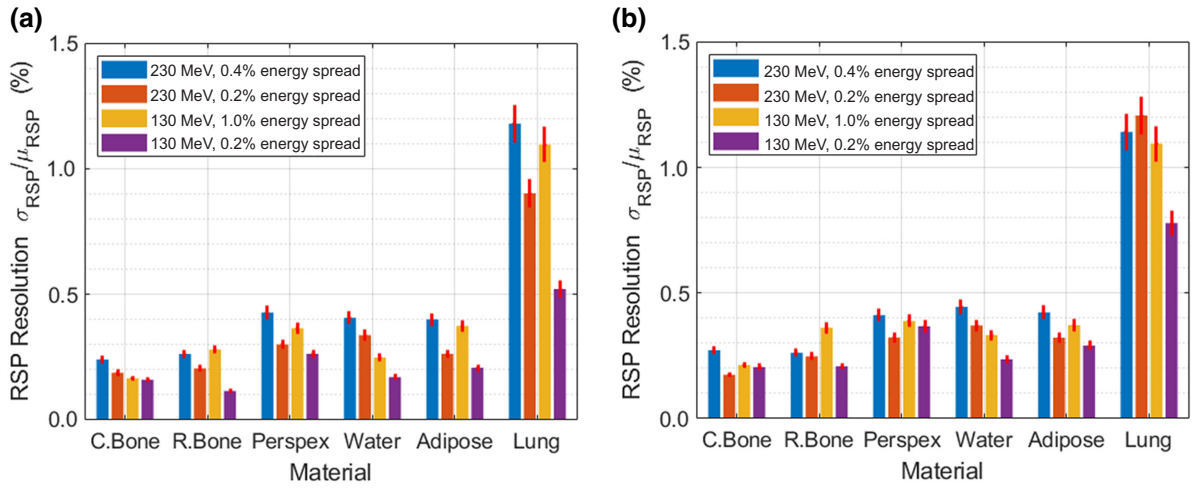

FIG. 5. RSP values determined by simulation for imaging of cortical bone, rib bone, PMMA, water, adipose, and lung tissue using 130- and 230-MeV pencil beams with energy spreads of a treatment beam (0.4% at 230 MeV and 1.0% at 130 MeV) and of 0.2%, simulated for a perfect energy detection resolution (left) and for the residual energy detection resolutions in Table II (right). For both sets, we see an improvement in RSP resolution with a reduction in beam energy spread, at both energies studied.

resolution (with path tracing accuracy) is critical for determining which residual energy provides the optimal RSP resolution.

V. DISCUSSION

Through assembling all results in Fig. 5, we see that the ideal operating condition for RSP resolution in pCT is with the smallest-possible energy spread in the initial proton beam, with energy choice dependent on the tissue scanned and the method used for residual energy measurement.

The reduced beam energy spread consistently produces results of between 60% and 100% of the RSP resolution obtained for the beam energy spread of a treatment beam, for all materials studied.

While a nonzero energy measurement uncertainty serves to blur the improvement from a smaller beam energy spread, the results in Fig. 5(a) show this clearly.

Indeed, by separating out the results for a perfect and nonperfect energy measurement [in Figs. 5(a) and 5(b), respectively], we can decouple the energy measurement resolutions in Table II from our results. Hence, we determine a natural improvement in RSP resolution at lower beam energies (which we associate with the increased energy absorption in the phantom, leading to a clearer indication of depth traveled), which is then counteracted by the resolution of the energy measurement method. Therefore, for other energy measurement methods, we expect the optimal beam energies to be determined by the energy resolution profile of that method.

However, we note that the lower the residual energy, the higher the dose absorbed by the patient. At 130 MeV, this dose may increase by 50% over that at 230 MeV. While there may be some improvement in RSP resolution for some materials at this lower energy, it is unlikely to justify the higher dose.

It is also worth noting that, although we are optimizing for RSP resolution, the spatial resolution will be adversely affected by lowering the scanning energy due to increased multiple scattering within the phantom. The balance of RSP and spatial resolutions should be factored into treatment planning, though the reduction of beam energy spread will be of benefit at any energy.

VI. CONCLUSION

These simulations show that the RSP resolution of pCT imaging in the organic materials studied can be improved by up to 40% by reducing beam energy spread to (an achievable) 0.2%. While further improvements (particularly for lung tissue) could be made by also choosing a suitable scanning (i.e., residual) energy, this gain would be coupled with effects from spatial resolution and patient dose. Though these results are obtained for a specific scanning hardware, we expect the improvements from reduced beam energy spread to persist for all other pCT imaging technologies.

Through decoupling our results from the energy measurement method [in Fig. 5(a)], we find that the different materials studied exhibit between 5% and 45% better RSP resolutions at low scanning energies (due to a higher fraction of the energy being absorbed). However, this improvement is much more consistent and pronounced (with between 45% and 65% reduction in RSP resolution) when the energy measurement resolution is ignored.

Hence, we expect a beam optimized for RSP resolution in a pCT scan to have the optimal energy for the residual direction and energy tracking to operate, and have a

minimal beam energy spread, with the latter demonstrated at PSI (in Sec. II) to be readily achievable in existing machines. The latter, readily implementable change should result [as in Fig. 5(b)] in RSP resolution improvements of up to 40% for cortical and rib bone, water, adipose, and lung tissue.

ACKNOWLEDGMENTS

This work is sponsored by the STFC Cockcroft Institute (Core Grant No. R120969/D0101). This work is supported partly by EPSRC Grant No. EP/R023220/1.

[1] G. Poludniowski, N. M. Allinson, and P. M. Evans, Proton radiography and tomography with application to proton therapy, Br. J. Radiol. **88**, 20150134 (2015).

[2] R. P. Johnson, Review of medical radiography and tomography with proton beams, Rep. Prog. Phys. **81**, 016701 (2017).

[3] E. Schnell, S. Ahmad, and T. de la Fuente Herman, Commissioning of a relative stopping power to Hounsfield unit calibration curve for a mevion proton radiation treatment unit, AIP Conf. Proc. **1747**, 110004 (2016).

[4] J. Dickmann, C. Sarosiek, V. Rykalin, M. Pankuch, G. Coutrakon, R. Johnson, V. Bashkirov, R. Schulte, K. Parodi, G. Landry, and G. Dedes, Proof of concept image artifact reduction by energy-modulated proton computed tomography (EMPCT), Phys. Med. **81**, 237 (2021).

[5] Performed as part of the INSPIRE Transnational Access (TNA) programme, sponsored by European Union Horizon 2020 research and innovation programme grant agreement 730983.

[6] M. Schippers, J. Duppich, G. Goitein, E. Hug, M. Jermann, A. Mezger, and E. Pedroni, in *Proc. of 18th International Conference on Cyclotrons and Their Applications (CYCLOTRONS 07), Giardini Naxos, Messina, Italy, 1-5 October 2007*, International Conference on Cyclotrons and Their Applications No. 18, edited by D. Rifuggiato (JACoW, Geneva, Switzerland, 2007), p. 15.

[7] S. Psoroulas, D. Meer, E. Oponowicz, and H. Owen, Mean excitation energy determination for Monte Carlo simulations of boron carbide as degrader material for proton therapy, Phys. Med. **80**, 111 (2020).

[8] T. Bortfeld and W. Schlegel, An analytical approximation of depth—dose distributions for therapeutic proton beams, Phys. Med. Biol. **41**, 1331 (1996).

[9] G. Poludniowski, N. M. Allinson, and P. M. Evans, Proton computed tomography reconstruction using a backprojection-then-filtering approach, Phys. Med. Biol. **59**, 7905 (2014).

[10] M. Esposito, C. Waltham, J. T. Taylor, S. Manger, B. Phoenix, T. Price, G. Poludniowski, S. Green, P. M. Evans, P. P. Allport, S. Manolopulos, J. Nieto-Camero, J. Symons, and N. M. Allinson, Pravda: The first solid-state system for proton computed tomography, Phys. Med. **55**, 149 (2018).

[11] D. Hansen, J. Seco, T. Sangild, S. Rensen, J. Rgen, B. Petersen, J. Wildberger, F. Verhaegen, and G. Landry, A simulation study on proton computed tomography (CT) stopping power accuracy using dual energy CT scans as benchmark, Acta Oncol. **54**, 1638 (2015).

[12] G. Landry, F. Dörringer, S. Si-Mohamed, P. Douek, J. F. P. J. Abascal, F. Peyrin, I. P. Almeida, F. Verhaegen, I. Rinaldi, K. Parodi, and S. Rit, Technical note: Relative proton stopping power estimation from virtual monoenergetic images reconstructed from dual-layer computed tomography, Med. Phys. **46**, 1821 (2019).

[13] J. Taylor, C. Waltham, T. Price, N. Allinson, P. Allport, G. Casse, A. Kacperek, S. Manger, N. Smith, and I. Tsurin, A new silicon tracker for proton imaging and dosimetry, Nucl. Instrum. Methods Phys. Res., Sect. A **831**, 362 (2016).

[14] M. Granado-González, C. Jesús-Valls, T. Lux, T. Price, and F. Sánchez, A novel range telescope concept for proton CT therapy, ArXiv:2109.03452 (2021).